# Thermophoresis as a technique for separation of nanoparticle populations in microfluidic devices: a numerical study

Ane Errarte[1], Alain Martin-Mayor[1], Maialen Aginagalde[1], Ibon Iloro[3,5], Esperanza Gonzalez[2], Juan Manuel Falcon-Perez[2,3,4], Felix Elortza[3,5], M. Mounir Bou-Ali[1]

[1]Manufacturing Department, MGEP Mondragon Goi Eskola Politeknikoa, Loramendi 4 Apartado 23, 20500 Mondragon, Spain. mbouali@mondragon.edu

[2]Exosome Laboratory. CIC bioGUNE, Bizkaia Technology Park, 801 building, 48160, Derio, Spain.

[3]Centro de Investigación Biomédica en Red de Enfermedades Hepáticas y Digestivas (CIBERehd).

[4]Ikerbasque, Basque foundation for science, Bilbao, Spain

[5] Proteomics Platform, CIC bioGUNE, ProteoRed-ISCIII, Bizkaia Technology Park, 800 Building, Derio, Spain.

***Keywords****: Nanoparticle, Thermodiffusion, Thermophoresis, Microdevice, Separation, Stratification*

## Abstract

This paper presents numerical studies of thermophoresis approach for separation of nanoparticles in liquid media. We simulated the thermophoresis process to test it as a method of separation of particles in suspension. At the same time, the specific software was appraised to establish whether it would meet the computational challenge. Then, a microfluidic device designed to separate different populations of nanoparticles using thermal gradients was conceptualised. We used a theoretical nanoparticle population with diameters ranging between 40 and 250 nm. A temperature gradient was set up between the walls of the microdevice to control the trajectories of the particles. Different geometrical models, temperature gradients and entry flows were simulated to analyse their effect on the separation of nanoparticle populations. On the basis of our results, we formulated a proposal for construction of efficient nanoparticle separation device.

## Introduction

Since the first observations of thermodiffusion reported by Ludwig [1] and Soret [2] at the end of the 19$^{th}$ century, many studies of this phenomenon have been carried out. Thermodiffusion, or Ludwig–Soret effect, is a process of generation of concentration gradient induced by a thermal gradient. This phenomenon is an additional transport mechanism on top of molecular diffusion. The molar flux of component $i$ in a multicomponent mixture can be represented by Eqn. (1)[3].

$$\vec{J}_i = -\rho\left(\sum_{k=1}^{n-1} D_{ik}\nabla \mathrm{c}_k + D'_{T,i}\,\nabla T\right) \qquad i = 1, \dots n-1, \tag{1}$$

where $\vec{J}_i$ is the molar flux of component $i$, ρ is the density of the mixture, $D_{ik}$ is the molecular diffusion tensor and $\nabla \mathrm{c}_k$, the spatial gradient of mass fraction of the component $k$. $D'_{T,i}$ is the thermodiffusion coefficient of the component $i$, $T$ is the temperature and $\nabla T$, the spatial temperature gradient across the mixture.

The representative magnitude of the thermodiffusion phenomenon is the Soret coefficient. In a binary system, this coefficient is defined as the ratio of the thermodiffusion and the molecular diffusion coefficient, $S_T = D_T/D$.

When a colloidal suspension is placed in a thermal gradient, the dispersed particles move to the cold or hot side of the field at a uniform trawl speed $v_{T,i} = -D'_{T,i}\nabla T$ [4]. Depending on the sign of the thermodiffusion coefficient, $D'_{T,i}$ , the system reaches a steady-state of concentrations (Eqn. (2))[5]:

$$\frac{\partial c_i}{\partial x} = S'_{T,i}\frac{\partial T}{\partial x} \tag{2}$$

The Soret coefficient can be positive or negative, contingent on the direction of the bulk component migration. When $S'_{T,i}$ > 0, the suspension is thermophobic; the densest component moves towards the cold side while the less dense component migrates to the hot side. The less common and opposite tendency is defined as thermophilic. As a consequence of the displacement of particles, a concentration gradient is generated. Thus, another flux is generated in the opposite direction due to the molecular diffusion, which tends to homogenise the mixture.

Recently, thermal diffusion as a transport mechanism has become the subject of growing interest in the scientific community as it plays an important role in many research areas. Multicomponent mixtures and separation methods [6], combustion processes [7] and geological characterisation [8] are just some of the fields we could mention. The European Space Agency has collaborated in the design of the Diffusion and Thermodiffusion Coefficients in ternary Mixtures project (DCMIX), focused on the research of mass transport in ternary mixtures, including various experiments under microgravity conditions [9-10]. Thermodiffusion has also been proposed as a possible mechanism for transport in biological systems [11]. Many reports point out that understanding thermodiffusion might improve our ability to control such systems

[12] and help us exploit its potential in the characterisation of biological fluids [13]. Recently, some preliminary studies have suggested using thermodiffusion as a control parameter in separation processes in micro-scale devices [14–16].Nevertheless, these last works show the separation of a complete population of nanoparticles from a bulk fluid, never showing a population separation in a liquid media (population separation is presented for a gaseous medium in [15]).

The focus of our project was to obtain a fast, efficient and inexpensive method to purify and separate different populations of nanoparticles. To this end (and to the best of our knowledge, for the first time), a microfluidic device using thermal gradients was designed to obtain nanoparticle separation by size in a liquid medium.

## Numerical analysis

Previous studies have demonstrated that diffusion [17] and thermodiffusion [16], [18–20] are valid techniques for separation of binary mixtures, on a micro- and macro-scale, and proven that ANSYS Fluent 16.0 [21–23] is appropriate software to simulate those processes.

To study the thermophysical process of separation and purification of subpopulations of nanoparticles within complex suspensions, several simulations were performed using ANSYS Fluent 16.0. First, we made a model validation and second, the nanoparticle populations' suspension was simulated. In all cases, the capacity of the software to simulate the thermodiffusion phenomenon was demonstrated, and the same steps were followed: the flow domain definition, the numerical model definition, obtaining the results and discussion report.

### Thermophoresis model validation

The first simulation was performed to determine the precision of the software in the simulations by injecting a particle suspension. In particular, the microdevice presented here was utilised to analyse the thermophoretic displacement of polystyrene (PS) suspended in 100 mM NaCl. Thus, the microdevice was simulated, and the results were compared to those published by Vigolo *et al.*[24].

#### 1- Flow domain

The geometry of the computational domain was designed using SolidWorks programme, according to the dimensions given by Vigolo *et al.* [24] for a rectangular channel of 25-µm height, 75-µm width and 50-mm length. Once completed, the domain model was imported to ANSYS Meshing 16.0, where a fine hexahedral mesh was built. The mesh had approximately 3 million elements and was finer near the walls, the inlet and the outlet of the channel.

## 1- Numerical model

The case was resolved using the Euler-Lagrange approach, where the fluid phase is considered a continuum and the dispersed phase is considered the secondary phase constituting a small fraction of the volume.

For the base fluid, a laminar flow was set. The dispersed particles in the laminar flow were tracked employing the Eulerian-Lagrangian Method using the Discrete Phase Model (DPM) in a two-way interaction, which computes the trajectories of each particle in a Lagrangian frame. During the tracking, the programme calculates the trajectory, considering the drag force per unit particle mass ($F_{drag}(\vec{u} - \vec{u}_p)$), the additional acceleration force $\vec{F}$ and properties such as the dynamic viscosity $\mu$, the particle and fluid density and velocity ($\vec{u}$ and $\vec{u}_p$). The trajectory of each individual particle is determined at specific time intervals by the equation of particle motion, using an integrating method. The motion of the particle can be defined by Eqn. (3):

$$F_{drag}(\vec{u} - \vec{u}_p) + \frac{\vec{g}(\rho_p - \rho)}{\rho_p} + \vec{F} = \frac{d\vec{u}_p}{dt} \quad (3)$$

The continuous and discrete phases were assumed to exchange heat, mass and momentum; the interactions between particles were not considered since the particle volume fraction was relatively small, around 1%. Furthermore, given that the displacement of the particles was created by thermal gradients, the thermophoretic force was included in the simulation.

The thermophoretic force is a transport phenomenon, where the particles produce different responses when a temperature gradient is applied. The coefficient representing this force is defined by Eqn. (4), and it was entered into the programme employing a User-Defined Function (UDF)[15].

$$D'_{T,i\,fluent} = 6\pi \cdot \mu \cdot T \cdot D'_{T,i\,exp} \cdot \frac{D_p}{2} \quad (4)$$

where $D'_{T,i\,exp}$ is the experimental thermodiffusion coefficient and $D_p$ is the particle diameter. Thus, the program calculates the thermodiffusion coefficient for each of the tracked particles.

Moreover, submicron particles in a shear field experience a lift force perpendicular to the direction of the flow. This shear lift originates from the inertia effects in the viscous flow around the particle. For small Reynolds-number flows, it can be defined by Eqn.(5)[25].

$$\vec{F} = \frac{2K\nu^{\frac{1}{2}}d_{ij}}{Sd_p(d_{lk}d_{kl})^{\frac{1}{4}}}\left(\vec{u} - \vec{u}_p\right), \quad (5)$$

Where $K$ = 2.594, $\nu$ is the kinematic viscosity, $d_{ij}$ is the deformation tensor and $S$ is the ratio of particle density to fluid density.

Once all forces were established, a surface injection of 477-nm PS particles from the inlet of the device at a temperature of 298.16 K was set. The particles in suspension were defined as inert at a mass fraction concentration of 1%, and their velocity was fixed at the same velocity as that of the carrier fluid.

Apart from defining the physical phenomenon for the case, it is necessary to define the properties of the two materials in the simulation, the aqueous 100 mM NaCl solution and the PS particles [4], [26-27]. The fluid and the particles entered with a velocity of 90 µm/s. Then, a temperature gradient between the lateral walls was applied (a 2.42-K difference); the temperature at the right wall was 304.37 K, and at the left wall, 301.95 K. The top and bottom walls were defined as adiabatic stationary walls without slip. Thus, any particles hitting a wall are reflected and escape when the outlet is reached [28].

**1- Results and discussion**

In our numerical model, all the PS particles move towards the cold side. Figure 1 presents our results and those of the experimental study published by Vigolo *et al.*[24]. Figure 1A shows the fluorescence images demonstrating the accumulation of particles at the cold side and Figure 1B, the patterns obtained by our numerical simulation. The displacement profiles of PS particles in the two studies are similar.

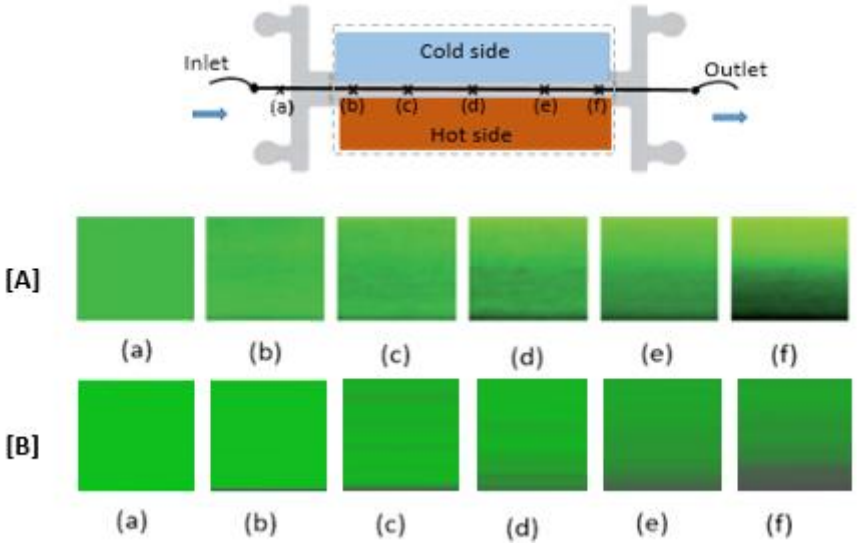


*Figure 1: Displacement of particles towards the cold side for different locations in the channel. Comparison between experimental results published by Vigolo et al.*[24] *[A] and the results of our simulation [B]. Reproduced from ref. 43 with the permission of the Royal Society of Chemistry.*

The concentration distributions obtained in the two studies are presented in Figure 2.

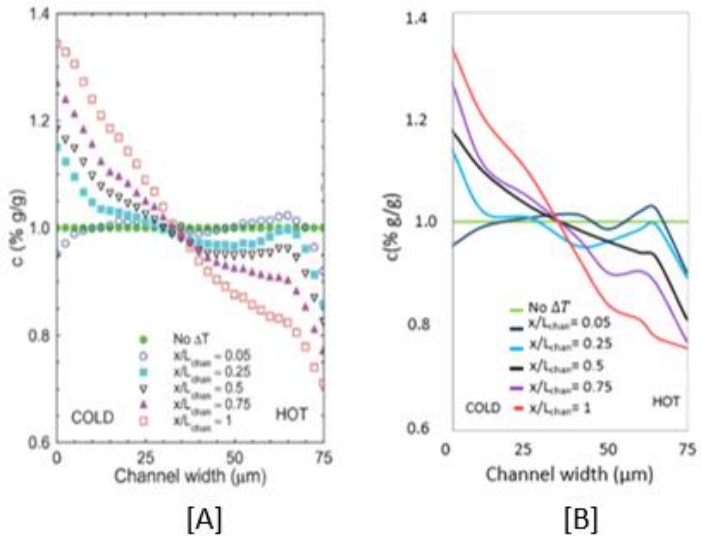


*Figure 2: Comparison of concentration profiles: experimental results published by Vigolo et al.*[24] *[A] and the numerical results of this work [B]. Reproduced from ref. 43 with the permission of the Royal Society of Chemistry.*

Even though there are some slight differences between the separation profiles obtained in our simulation and the experimental studies of Vigolo *et al.* [24], the results are remarkably similar. The observed differences might be due to the mesh configuration and material properties value used in the simulation.

In summary, the use of thermodiffusion method as a particle separation technique was validated. Moreover, the correct functioning of the software and model were verified.

## The size based separation and purification of nanoparticles

Once the software and the thermophoresis as a separation technique were validated, several simulations were performed to define the nanoparticle motion trajectories under different conditions. After analysis of the results, the most suitable scenario was chosen for the final device design.

### 1- Flow domain

In the first design, the microdevice consisted of a bidimensional rectangular channel, 30-mm long, with a 1-mm long cytometer in its entrance. The main objective of the cytometer design was to limit the inlet area and apply the most homogeneous gradient possible to the whole sample. The examined values of the dispositive height H were 50 µm, 100 µm, 200 µm, 400 µm, 800 µm and 1600 µm. The height of the cytometer was defined as h. The relationship between H and h was maintained in all simulations, the latter being 1/5 of the total height (Figure 3).

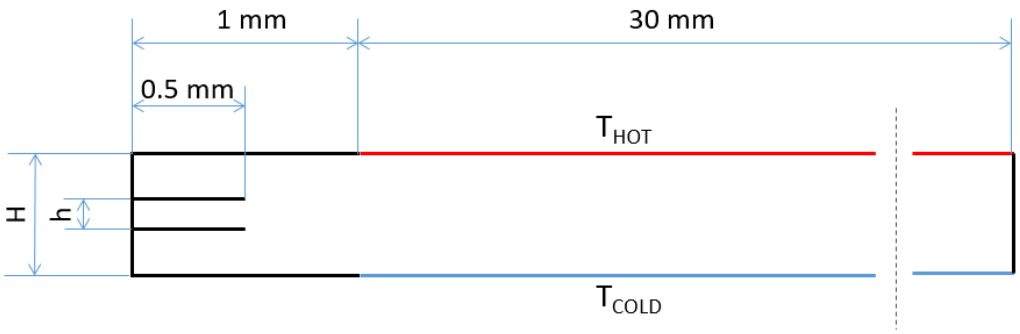


*Figure 3: Flow domain used to analyse the behaviour of nanoparticles in the presence of a thermal gradient.*

### 2- Numerical model

As in the PS particle simulation, the cases were solved using the Euler-Lagrange approach. For the PBS (Phosphate Buffered Saline) base fluid, a laminar flow was set. The nanoparticles were injected, and trajectories were calculated using the DPM in a two-way interaction. In these simulations, the thermophoretic force and lift force were the same as in the numerical model of the PS particles simulation.

The PBS suspension of nanoparticles (size from 40 to 250 nm) was entered through the central cavity of the cytometer, and the PBS through the superior and inferior cavities. The particle injections were set using the DPM properties. An injection entered from the surface of the central inlet was established; the inert particles were injected at room temperature. The velocity of the particles was the same as that of the carrier fluid; this varied depending on the height of the device.

Various thermophysical and transport properties of the carrier fluid necessary to perform the numerical analysis were determined at the Fluid Mechanics Laboratory of Mondragon University. The density, viscosity, thermal expansion coefficient and thermodiffusion coefficients were obtained although only the first two parameters were used in the study.

The first and most important step in the characterisation of properties is the sample preparation, for which a Gram VXI-310 precision balance was used. The measurement of the density and thermal expansion coefficient was carried out using an Anton Paar DMA 5000 vibrator-type densitometer with U- form quartz tube sensor. The viscosity was examined employing an AMVn microviscometer of falling ball principle (Anton Paar AMV). A more detailed description of the determination of thermophysical and transport properties can be found in the study of Lapeira *et al.*[29].

For each property, at least 3 tests were performed to obtain robust results with deviations not exceeding 6%. However, some properties could not be determined in the laboratory but were needed to define the materials used in the analysis. The values of these properties were found in the literature. The values corresponding to the nanoparticles are from nano-size biological molecules, since this device could be directly used in the separation of biomolecules offering all advantages mentioned in the introduction in front of nowadays-used techniques. All the properties used to define the materials for ANSYS Fluent 16.0 simulation are shown in Table 1.

*Table 1: PBS and nanoparticle properties at 25ºC* [4], [30–32].

| **Material** | **PBS** | **Nanoparticles** |
|---|---|---|
| Density (kg/m$^3$) | 1003.98 (this work) | 1160.00 [31] |
| Specific heat (J/kg · K) | 4182.00 [26] | 3739.60 [33] |
| Thermal conductivity (W/m·K) | 0.60 [26] | $5.14 \cdot 10^{-1}$ [34] |
| Thermal expansion (K$^{-1}$) | $26.99 \cdot 10^{-5}$ (this work) | - |
| Viscosity (kg/m·s) | $92.05 \cdot 10^{-5}$ (this work) | - |
| Molecular weight (g/mol) | 18.15 [26] | - |
| Reference temperature (K) | 298.16 | - |
| Thermophoretic coefficient (m$^2$/s·K) | - | $1.70 \cdot 10^{-12}$ [4] |

The nanoparticles thermophoretic coefficient was entered using the UDF defined in the previous simulation, see Eqn. (4). To create the temperature gradient, an 8-K temperature difference was applied between the top and the bottom walls. The top wall was heated to 302.16 K, and the bottom wall was maintained at 294.16 K. The inlet and outlet were kept at room temperature, and the tip of the cytometer was maintained at 298.16 K, without applying the temperature gradient. As we are simulating a particle suspension, it is necessary to define the behaviour of

particles when hitting any of the defined geometrical domains. The particles hitting any of the walls would be reflected and escape after reaching the outlet.

### 3- Results and discussion

To analyse the separation of nanoparticle populations, different flows of sample and PBS were simulated. The parameter $f_q = Q_c/Q_T$ represents the relationship between the flow in the central channel of the cytometer and the total flow. In this study, the values of $f_q$ were predefined as 0.2, 0.1, 0.05 and 0.025 for total entry flow ($Q_T$) of 50, 100 and 200 ml/min for each channel height. Therefore, for the heights of 50, 100 and 200 µm, 12 simulations were performed, using all the combinations of $f_q$ and total flows. However, for the cases of 400, 800 and 1600 µm only $f_q$= 0.025 was simulated for all total flows.

In all cases, the particles moved towards the cold wall, but not all the conditions were suitable for the separation of the particles into different populations. With the height of 50 µm, no separation was achieved in any of the cases, and the height of 400 µm did not separate populations when the total flow was 200 ml/min. Furthermore, the device of 800-µm height did not separate the vesicles for entry flows of 200 ml/min and 100 ml/min, and with the height of 1600 µm, the device had to be longer to achieve separation.

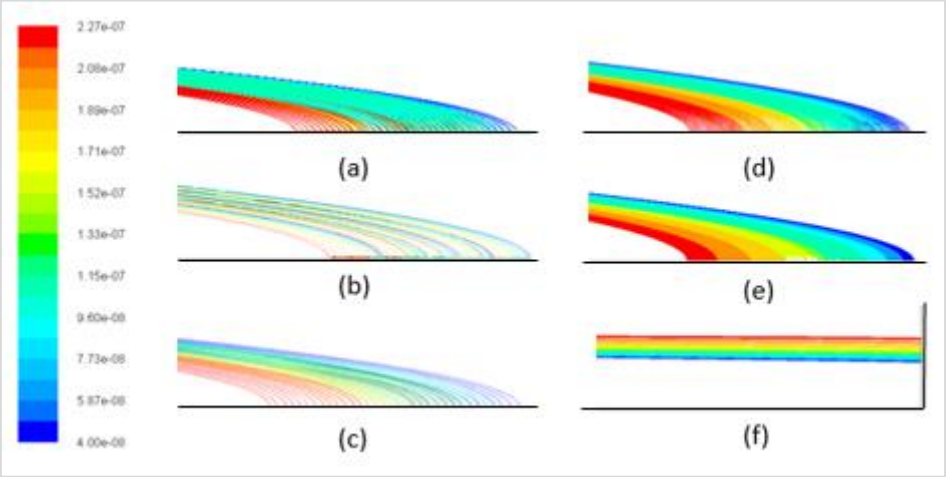


*Figure 4: Particle precipitation profiles in the cold wall obtained in different simulations for an 8 K temperature difference. (a) height of 50 µm, $Q_T$ of 50 ml/min and $f_q$ of 0.05. (b) 100-µm height, 50 ml/min $Q_T$ and $f_q$ of 0.05. (c) 200-µm height, 200 ml/min $Q_T$ and $f_q$ of 0.025. (d) 400-µm height, 100ml/min $Q_T$ and $f_q$ of 0.025. (e) 800-µm height, 50 ml/min $Q_T$ and $f_q$ of 0.025. (f) 1600-µm height, 50 ml/min $Q_T$ and $f_q$ of 0.025.*

As can be seen in Figure 4, the particles were stratified in response to the temperature gradient, reaching the cold wall after different intervals depending on their size. Red colour lines represent the displacement paths of the biggest size particles, orange and yellow colour represent medium particles, and green and blue ones' smallest particles. The biggest particles

reached the cold wall first and the smallest particles, last. To examine this phenomenon, the particle trajectory was determined for each case, defining the first and last position at reaching the bottom wall and measuring the whole precipitation zone. The stratification degree was calculated as the ratio between the precipitation zone of the biggest particles and the whole precipitation zone. Finally, the aspect ratio parameter was defined as the relationship between the distance from the inlet to the last particles precipitated and the height of the channel. Figure 5 shows the relationship between the stratification degree and the original Reynolds number multiplied by the aspect ratio (a).

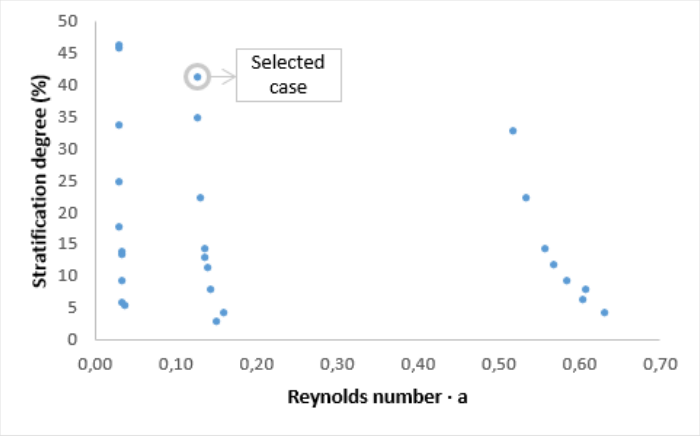


*Figure 5: The stratification degree of nanoparticles against the Reynolds number multiplied by the aspect ratio, for an 8 K temperature difference between the top and bottom walls.*

In Figure 5, three different series can be observed, depending on the Reynolds number that defines the laminar flow in each example. The first series corresponds to the 50 ml/min flow, the second to the 100 ml/min and the third, to the 200 ml/min flow. Moreover, the cases in which the inlet flow ratio $f_q$ is larger coincide with the top cases in these three groups, while the smallest ratios correspond to the cases at the bottom of the plot.

The lower the Reynolds number and the higher the flow relationship $f_q$, the higher was the obtained stratification degree. The separation improves with increasing degree of stratification. As seen in Figure 7, the highest stratification had the lowest Reynolds number, and the separation does not improve when this number increases. Thus, the separation seems significant only for small Reynolds numbers and is almost non-existent for large Reynolds numbers.

The case and conditions chosen for population extraction analysis obtained one of the largest stratification degrees observed. However, for this approach, other factors, such as time, were

also taken into account. As the entry flow and the temperature difference between the top and bottom walls were the same in all cases, the separation time increased for the largest channel heights. The 400-µm height and 100-ml/min entry flow were selected for population extraction simulations, with a stratification time of approximately 100 min (Figure 6).

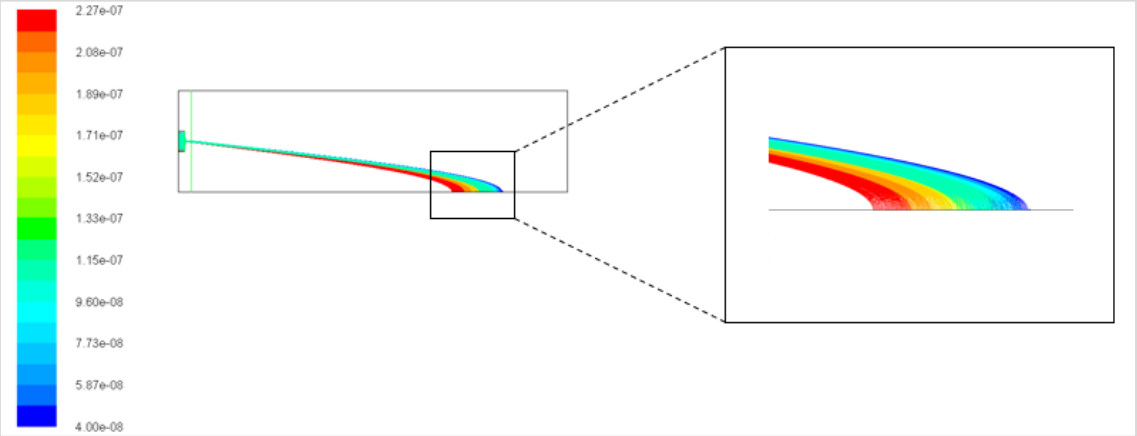


*Figure 6: Particle displacement towards the cold wall. Results for the case with a height of 400 µm and 100-ml/min entry flow.*

As we mentioned above, all the particles moved towards the cold wall but at different velocities. Along the channel, the particles were stratified due to the temperature gradient; the first particles to reach the cold wall were the biggest. One of the points emphasized by the authors of [15], where thermophoresis of a single population of nanoparticles in fluids is also studied, is that the gravitational force does not affect the particle trajectory even if it is part of the force balance equation (3). In the mentioned work, particles of 1 µm are entered in a microfluidic platform of 8 mm length with an inlet velocity of 1 mm/s. In this case, taking into account the fast velocity condition applied in the inlet, the gravitational force does not affect in the particles trajectory. However, in our case low inlet velocity conditions are set to obtain the population separation. We saw, that in this case, based on the conditions we imposed the gravitational force helps in the stratification of the nanoparticles, due to the same action direction of the thermophoretic force.

Taking into account the separation profile obtained in the case shown in Figure 6, an exit was placed in the cold wall to extract the biggest particles.

The outlet in the inferior wall was located in the precipitation zone of the biggest vesicles. The boundary conditions of this outlet were adjusted for different separations. Various simulations were performed with different flows from each outlet. The inferior outlet was set at 30%, 20%, 15%, 10% and 5% of the total entry flow, with the remaining flow directed through the general outlet in each case. For each simulation, the velocity at the inlet was adjusted to direct the

particles towards the outlet. The best result was obtained when the flow extracted from the inferior outlet was 5% of the total flow (Figure 7).

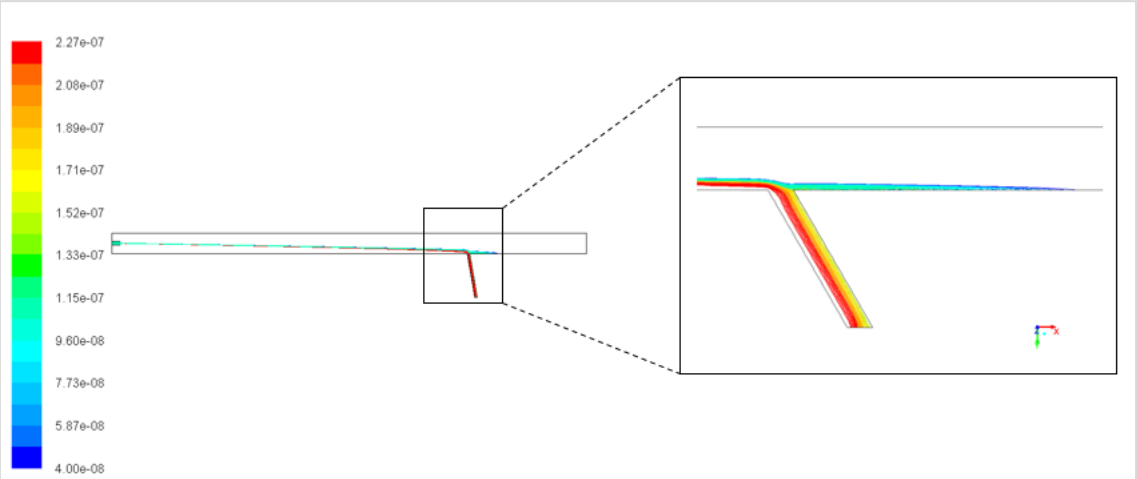


*Figure 7: Extraction of half of the vesicle population by the outlet located in the cold wall.*

Modulating the inlet velocity and the exit flow percentage controls the extraction; these values can be adjusted to extract only the desired populations. The bigger the flow extracted from the inferior outlet, the greater is the force what exerted on the particles in that orifice; therefore, more particles are extracted.

Different correlations were examined to determine the conditions needed to separate different populations (Table 2). Nevertheless, other conditions could be used, or the sample could be re-applied to extract different populations.

*Table 2: Boundary conditions determination for different population separations for a temperature gradient of 8 K.*

| **Inferior exit Extraction diameter range (nm)** | **Superior exit Extraction diameter range (nm)** | **Cytometer entry velocity (µm/s)** | **PBS entry velocity (µm/s)** | **Inferior outlet flow (% of total flow)** |
|---|---|---|---|---|
| 250-200 | 40-200 | $5.21 \cdot 10^{-1}$ | 5.70 | 5.00 |
| 250-150 | 40-150 | $5.21 \cdot 10^{-1}$ | 5.50 | 5.00 |
| 250-100 | 40-100 | $5.21 \cdot 10^{-1}$ | 5.30 | 5.00 |

If only one exit is set in the cold wall, two populations can be separated, the biggest particles exiting the channel via the inferior outlet, and the remaining particles, leaving through the principal channel. In the second simulation, a second exit was made, and 5% of the total flow was defined for each of the two inferior outlets. The biggest particles were extracted from the first outlet while the smallest exited from the second inferior outlet. The separations obtained for one and two exits were the same. The only difference was that in the first simulation, the

smallest particles were obtained from the central channel exit and in the second, from the other inferior outlet. In the latter case, the vesicle population was more concentrated.

The third simulation was performed to separate three different populations. Two exits were set, 7% of the total flow was defined for the first outlet and 2%, for the second. Three different populations were separated. However, the boundary conditions set here were not appropriate for the experimental trials; thus, one of the outlets had to be forced to the limit (Figure 8).

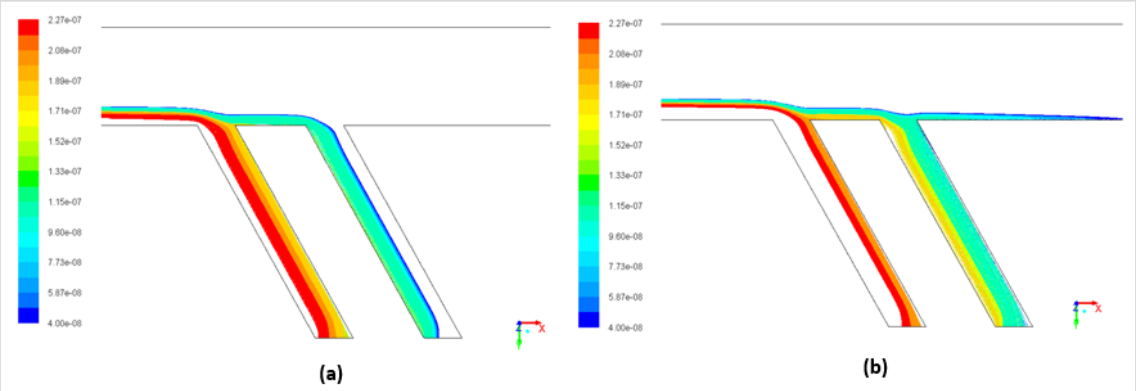


*Figure 8: Extraction of particles in the two-outlet device. (a) Extraction of three populations. (b) Extraction of half of the population from each outlet.*

The results indicate that the simulation conditions are the key for the extraction, not the number of exits. By varying the inlet velocity and the outlet flow, the desired particle populations can be isolated. Thus, the final design proposed for the manufacture is a two-outlet device with 5% of the total flow in each outlet.

## Conclusions

The main aim of this paper was to analyse the potential of thermodiffusion method for the separation of nanoparticle populations in a bulk fluid. The behaviour of PS particles in thermal gradients has also been studied and validated.

We confirmed that thermodiffusion is a valid technique for substance separation. The temperature gradient applied between the microdevice walls gradient were the main parameters determining the degree of separation (better separation for larger gradients). Apart from validation of the thermodiffusion phenomena, the suitability of the software tools was analysed. The results indicated that the ANSYS Fluent programme is appropriate for simulating the separation of binary mixtures and molecular suspensions.

For the separation of nanoparticle populations, thermodiffusion is an easy, fast and cheap technique in comparison with the currently prevalent methods; it also uses small sample volumes. Under the analysed conditions, all particles moved towards the cold side of the device; the first particles reaching the cold wall were the biggest, and the last were the smallest. We observed the best separation in cases with a small Reynolds number and large difference between the entry flow and the total flow. We also found that for high Reynold numbers, the entry flow did not affect the quality of separation.

After examining the devices with inferior wall exits, we concluded that the best results were achieved using the device with two outlets located in the bottom surface. Two concentrated populations were obtained under these conditions; if more populations are required, the process can be repeated (reintroducing the sample and adapting the working parameters).

We believe that this new methodology can be of particular interest to the biomedical sector; nanovesicles such as exosomes are attracting increasing attention as a source for biomarkers discovery, with an important role in the liquid biopsy. This new technology would enable a fast, efficient, cheap and easy purification of different populations. For this reason, all the techniques and geometries used in the analysis are summarised in the patent number P201631380 [35]. Our future studies will be focused on making and validating the exosome separation device.

## Acknowledgments

The Mondragon Goi Eskola Politeknikoa (MGEP) group thanks for the support of BG2015 (KK-2015/0000089), Research Groups (IT009-16) and MICROXOM (PI_2014_1_70) of the Basque Government and ATNEMFLU of MINECO (ESP2017-83544-C3-1-P).

## Bibliography

[1] C. Ludwig, “Diffusion zwischen ungleich erwärmten Orten gleich zusammengesetzter Lösungen,” *Sitz. Ber. Akad. Wiss. Wien Math-Naturw*, vol. 20, p. 539, 1856.

[2] C. Soret, “Au Piont De Vue Da Sa Concentration Une Dissolution Saline Primitevement Homogéne Dont Deux Parties Sont Portées a Des Températures Differentes,” *Arch. des Sci. Phys. Nat. Genéve*, vol. 3, pp. 48–61, 1879.

[3] P. Blanco, M. M. Bou-Ali, J. K. Platten, D. A. De Mezquia, J. A. Madariaga, and C. Santamaría, “Thermodiffusion coefficients of binary and ternary hydrocarbon mixtures,” *J. Chem. Phys.*, vol. 132, no. 11, 2010.

[4] R. Piazza and A. Parola, “Thermophoresis in colloidal suspensions,” *J. Phys. Condens. Matter*, vol. 20, no. 15, p. 153102, Apr. 2008.

[5] A. Mialdun and V. Shevtsova, “Communication: New approach for analysis of thermodiffusion coefficients in ternary mixtures,” *J. Chem. Phys.*, vol. 138, no. 16, 2013.

[6] J. K. Platten, M. M. Bou-Ali, and J. F. Dutrieux, “Enhanced Molecular Separation in Inclined Thermogravitational Columns,” *J. Phys. Chem. B*, vol. 107, no. 42, pp. 11763–11767, Oct. 2003.

[7] A. Eisner and D. E. Rosner, “Experimental Studies of Soot Particle Thermophoresis in Non-Isothermal Combustion Gases Using Thermocouple Response Techniques,” *Combust. Flame*, vol. 61, no. 2, pp. 153–166, 1985.

[8] T. J. B. Holland and R. Powell, “An internally consistent thermodynamic data set for phases of petrological interest,” *Journal of Metamorphic Geology*, vol. 16, no. 3. pp. 309–343, 2004.

[9] M. M. Bou-Ali *et al.*, “Benchmark values for the Soret, thermodiffusion and molecular diffusion coefficients of the ternary mixture tetralin+isobutylbenzene+n-dodecane with 0.8-0.1-0.1 mass fraction,” *Eur. Phys. J. E*, vol. 38, no. 4, pp. 0–6, 2015.

[10] D. Alonso de Mezquia, M. Larrañaga, M. M. Bou-Ali, J. A. Madariaga, C. Santamaría, and J. K. Platten, “Contribution to thermodiffusion coefficient measurements in DCMIX project,” *Int. J. Therm. Sci.*, vol. 92, pp. 14–16, Jun. 2015.

[11] D. Braun and A. Libchaber, “Thermal force approach to molecular evolution,” *Phys. Biol.*, vol. 1, no. 1, pp. P1–P8, Mar. 2004.

[12] R. D. Astumian, “Coupled transport at the nanoscale: The unreasonable effectiveness of equilibrium theory,” *Proc. Natl. Acad. Sci.*, vol. 104, no. 1, pp. 3–4, 2007.

[13] D. Braun and A. Libchaber, “Trapping of DNA by Thermophoretic Depletion and Convection,” *Phys. Rev. Lett.*, vol. 89, no. 18, p. 188103, Oct. 2002.

[14] R. Piazza, “Thermophoresis: moving particles with thermal gradients,” *Soft Matter*, vol. 4, no. 9, p. 1740, 2008.

[15] M. Eslamian and M. Z. Saghir, “Novel thermophoretic particle separators: Numerical analysis and simulation,” *Appl. Therm. Eng.*, vol. 59, no. 1–2, pp. 527–534, Sep. 2013.

[16] A. Martin-Mayor, M. M. Bou-Ali, M. Aginagalde, and P. Urteaga, “Microfluidic separation processes using the thermodiffusion effect,” *Int. J. Therm. Sci.*, vol. 124, no. July 2016, pp. 279–287, 2018.

[17] L. Florea *et al.*, “Adaptive coatings based on polyaniline for direct 2D observation of diffusion processes in microfluidic systems,” *Sensors Actuators, B Chem.*, vol. 231, pp. 744–751, 2016.

[18] J. A. Madariaga, C. Santamaria, H. Barrutia, M. M. Bou-Ali, O. Ecenarro, and J. J. Valencia, “Validity limits of the FJO thermogravitational column theory: Experimental and numerical analysis,” *Comptes Rendus - Mec.*, vol. 339, no. 5, pp. 292–296, 2011.

[19] P. Naumann, A. Martin, H. Kriegs, M. Larrañaga, M. M. Bou-Ali, and S. Wiegand, “Development of a thermogravitational microcolumn with an interferometric contactless detection system,” *J. Phys. Chem. B*, vol. 116, no. 47, pp. 13889–13897, 2012.

[20] Z. Liu, Z. Chen, and M. Shi, “Thermophoresis of particles in aqueous solution in micro-channel,” *Appl. Therm. Eng.*, vol. 29, no. 5–6, pp. 1020–1025, 2009.

[21] T. D. Canonsburg, “ANSYS Fluent Theory Guide,” vol. 15317, no. November, pp. 724–746, 2013.

[22] T. D. Canonsburg, “ANSYS FLUENT User’s Guide,” *ANSYS FLUENT User’s Guid.*, vol. 15317, no. November, p. 2498, 2013.

[23] T. D. Canonsburg, “ANSYS Meshing User ’ s Guide,” vol. 15317, no. November, pp. 724–746, 2013.

[24] D. Vigolo, R. Rusconi, H. a. Stone, and R. Piazza, “Thermophoresis: microfluidics characterization and separation,” *Soft Matter*, vol. 6, no. 15, p. 3489, 2010.

[25] A. Li and G. Ahmadi, “Dispersion and Deposition of Spherical Particles from Point Sources in a Turbulent Channel Flow,” *Aerosol Sci. Technol.*, vol. 16, no. 4, pp. 209–226, 1992.

[26] A. Fluent, “Ansys fluent 12.0 users guide,” *Ansys Inc*, vol. 15317, no. November, pp. 724–746, 2009.

[27] C. Minelli *et al.*, “Measuring the size and density of nanoparticles by centrifugal sedimentation and flotation,” *Anal. Methods*, vol. 10, no. 15, pp. 1725–1732, 2018.

[28] M. Bovand, S. Rashidi, G. Ahmadi, and J. A. Esfahani, “Effects of trap and reflect particle boundary conditions on particle transport and convective heat transfer for duct flow - A two-way coupling of Eulerian-Lagrangian model,” *Appl. Therm. Eng.*, vol. 108, pp. 368–377, 2016.

[29] E. Lapeira *et al.*, “Transport properties of the binary mixtures of the three organic liquids toluene, methanol, and cyclohexane,” *J. Chem. Phys.*, vol. 146, no. 9, 2017.

[30] T. D. Canonsburg, “ANSYS Fluent UDF Manual,” vol. 15317, no. November, pp. 724–746, 2013.

[31] M. Braibanti, D. Vigolo, and R. Piazza, “Does Thermophoretic Mobility Depend on Particle Size?,” *Phys. Rev. Lett.*, vol. 100, no. 10, p. 108303, Mar. 2008.

[32] B. J. Tauro *et al.*, “Comparison of ultracentrifugation, density gradient separation, and immunoaffinity capture methods for isolating human colon cancer cell line LIM1863-derived exosomes,” *Methods*, vol. 56, no. 2, pp. 293–304, 2012.

[33] N. L. Gershfeld, C. P. Mudd, K. Tajima, and R. L. Berger, “Critical temperature for unilamellar vesicle formation in dimyristoylphosphatidylcholine dispersions from specific heat measurements,” *Biophys. J.*, vol. 65, no. 3, pp. 1174–1179, 1993.

[34] Y. Sina, R. Nima, L. C. R., and V. D. Steven, “Variation of thermal conductivity of DPPC lipid bilayer membranes around the phase transition temperature,” *J. R. Soc. Interface*, vol. 14, no. 130, p. 20170127, 2017.

[35] M. M. Bou-Ali *et al.*, “Método de extracción de exosomas y dispositivo microfluídico de extracción de exosomas,” P201631380, 2016.